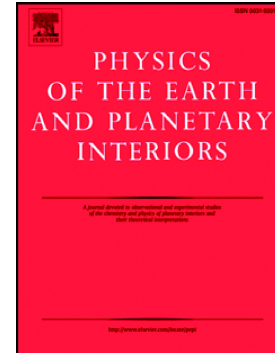


Journal Pre-proof

Seismic imaging of a mid-crustal low-velocity layer beneath the northern coast of the South China Sea and its tectonic implications

Pengxiang Zhou, Shaohong Xia, György Hetényi, Vadim Monteiller, Sébastien Chevrot, Jie Sun



PII: S0031-9201(20)30171-0

DOI: <https://doi.org/10.1016/j.pepi.2020.106573>

Reference: PEPI 106573

To appear in: *Physics of the Earth and Planetary Interiors*

Received date: 23 May 2020

Revised date: 23 August 2020

Accepted date: 30 August 2020

Please cite this article as: P. Zhou, S. Xia, G. Hetényi, et al., Seismic imaging of a mid-crustal low-velocity layer beneath the northern coast of the South China Sea and its tectonic implications, *Physics of the Earth and Planetary Interiors* (2018), <https://doi.org/10.1016/j.pepi.2020.106573>

This is a PDF file of an article that has undergone enhancements after acceptance, such as the addition of a cover page and metadata, and formatting for readability, but it is not yet the definitive version of record. This version will undergo additional copyediting, typesetting and review before it is published in its final form, but we are providing this version to give early visibility of the article. Please note that, during the production process, errors may be discovered which could affect the content, and all legal disclaimers that apply to the journal pertain.

© 2018 Published by Elsevier.

Seismic imaging of a mid-crustal low-velocity layer beneath the northern coast of the South China Sea and its tectonic implications

Pengxiang Zhou^{1,7}, Shaohong Xia^{1,2,3*}, György Hetényi⁴, Vadim Monteiller⁵, Sébastien Chevrot⁶, Jie Sun^{1,2,3*}

¹CAS Key Laboratory of Ocean and Marginal Sea Geology, South China Sea Institute of Oceanology, Chinese Academy of Sciences, Guangzhou, China

²Southern Marine Science and Engineering Guangdong Laboratory (Guangzhou), Guangzhou, China

³Innovation Academy of South China Sea Ecology and Environmental Engineering, Chinese Academy of Sciences, Guangzhou, China

⁴Institute of Earth Sciences, University of Lausanne, Switzerland

⁵Aix Marseille Univ., CNRS, Centrale Marseille, LMA, Marseille, France

⁶Observatoire Midi Pyrénées, GET, CNRS UMR 5563, Université Paul Sabatier, Toulouse, France

⁷College of Earth Sciences, University of Chinese Academy of Sciences, Beijing, China

*Corresponding author: Shaohong Xia (shxia@scsio.ac.cn); Jie Sun (sunjie@scsio.ac.cn)

Abstract

Low-velocity layers (LVLs) within the continental crust are usually closely associated with tectonic events, thus they may reflect ongoing processes or offer a chance to backtrack the evolutionary history. Mid-crustal LVLs have been reported in the northern coast of the South China Sea (SCS) by several geophysical studies, but the 3D distribution of LVLs in the whole coastal area is still poorly known. Here, we perform a receiver function study based on 67 broadband seismological stations. We use the common conversion point method to construct structures of the Moho as well as intra-crustal interfaces. We image sharp intra-crustal negative velocity gradients broadly distributed in the eastern Cathaysia block with depth increasing from ~10 km in the NW to 12~16 km in the SE. The corresponding amplitudes of these negative interfaces show variable values from -0.03 to -0.1, with an evidential trend of strengthening eastwards. We interpret these negative gradients as top of the LVL produced by accumulation of fluids from dehydration of the paleo-Pacific subduction plate. These mid-crustal LVLs tend to act as weak domains during continental rift and the lateral variation of the LVLs may be one possible reason explaining the along-strike variation in crustal stretching in the northern SCS rifted margin.

1 Introduction

The presence of intra-crustal low-velocity layers (LVL) can provide insights into the styles of crustal deformation and help to reconstruct the tectonic history. For example, the well-known mid-crustal LVL in Tibet was proposed to host channel flow, playing an important role in accommodating lithospheric deformations during extension (Nelson et al., 1996; Beaumont et al., 2001; Bao et al., 2015; Sun and Zhao, 2020), however, its geometry, connectivity and therefore importance are still debated (Hetényi et al., 2011). The shallow-angle, long-extent and low-velocity detachments observed in Himalaya (Schulte-Pelkum et al., 2005; Caldwell et al., 2013; Subedi et al., 2018), Central Andes (Yuan et al., 2000) and eastern America (Long et al., 2019; Marzen et al., 2019) indicate a fundamental deformation mode in continental collision zones. In several cases, intra-crustal LVLs result from accretionary complexes that reflect a tectonic transformation from subduction to extension (Smit et al., 2016). Or, intra-crustal LVLs can indicate a component akin to upper-middle crustal materials which have ‘frozen’ in the present-day stable crust, that dates back to craton formation (Zheng et al., 2009). Tending to form weak domains, inherited LVLs in continental crust can also impact later tectonic events, such as continental rifting. Pre-existing weak zones play an important role in controlling the location and duration of extension, rifting styles and post-rift evolution of continental margins (Sutra and Manatschal, 2012; Manatschal et al., 2015; Festa et al., 2019; Li et al., 2019; Zhao et al., 2020). Furthermore, structurally inherited weaknesses can control present-day intraplate deformation and seismicity by adjusting strain localization on a local scale (Tarayoun et al., 2019).

In South China, low-velocity/high-conductivity layers have been observed in deep seismic profiles (blue lines in Figure 1) (Liao et al., 1988; Xiong et al., 1991; Yin et al., 1999; Zhao et al., 2004; Zhang and Wang, 2007; Zhao et al., 2013), local seismic tomographic models (Zhang et al., 2018) and magnetotelluric soundings (Hu et al., 2017). The observed mid-crustal LVLs are rather flat and characterized by a P wave velocity of 5.5-6.0 km/s and thicknesses of 3 to 6 km. They have been interpreted as partial melt bodies, remnants of an ancient oceanic basin, or ductile shear zones. Through numerical simulation, Li et al., (2019) argues that LVLs could determine the width of the hyper-extended crust in the northern margin of the South China Sea (SCS). The LVLs may also be responsible for the present-day seismicity and historical earthquakes by providing an unstable crustal structure (Zou, 1998; Xu et al., 2006). Yet, due to limited coverage of the former 2D active source

seismic experiments (Figure 1), the distribution of the LVLs in the northern coast of the SCS is not clear.

Motivated by the numerous reports of mid-crustal LVLs and to address the above limitations, seismic waveforms recorded by 67 broadband seismological stations distributed in the northern coast of the SCS were used to analyze P-to-S receiver functions (RF). Taking advantage of RF's sensitivity to impedance contrasts, the goals of this research are to better constrain the spatial distribution of LVLs in the whole coastal area and discuss the nature and origin of the LVLs as well as their tectonic significance.

2 Tectonic overviews

Seismic stations used in this study are located in the Cathaysia block (Figure 1 and Figure 2), the convergence area of the Eurasian, Pacific and India-Australia plates. The Cathaysia and the Yangtze blocks collided and merged into the South China block (SCB) in the Neoproterozoic, forming the Jiangnan orogenic belt at their boundary (Zhao and Cawood, 1999, 2012; Li et al., 2002; Shu, 2012). After that, the united SCB experienced episodes of compression and extension (Shu, 2012). At present, it shows two dominant features: 1) the widespread Mesozoic granitoids and volcanic rocks (Figure 1), with the Early Yanshanian (180-140 Ma) igneous rocks mainly distributed in the continental interior and the Late Yanshanian (140-97 Ma) magmatism exposed along the southeastern coast (Zhou and Li, 2000), 2) the thinned lithosphere and crust whose thicknesses generally decrease towards the coast (Zhou et al., 2012; Shan et al., 2016). Such features are well explained by the flat subduction of the paleo-Pacific plate followed by slab break-off, foundering and roll-back during the Mesozoic (Li and Li, 2007; Suo et al., 2019). In early Mesozoic (ca. 250-190Ma), due to the flat-slab subduction of the paleo-Pacific plate, a ~1300-km-width orogenic belt was formed from SE to NW. During the early post-orogenic stage (ca. 190-150 Ma), the slab break-off and foundering caused the mantle upwelling and underplating. In the late Mesozoic (150 Ma-), slab rollback produced seaward migrating magmatism (Zhou and Li, 2000; Li and Li, 2007). The underplated basaltic magmas or hot mantle provided a significant amount of heat to partially melt the lower crust, generating granitic magmas and leaving behind dry mafic granulites (Zhou and Li, 2000). However, this model is still challenged by the geophysical observations, which inferred intercontinental extension induced by the lower-crustal and mantle delamination (He et al., 2013) or

asthenosphere upwelling (Deng et al., 2019). Notably, previous seismological studies mainly focused on the lithospheric and crustal structure, leaving the intra-crust poorly understood. Yet, the heterogeneous crustal interior may record much key information of the tectonic evolution.

The Mesozoic orogenic event led to the creation of NNE and ENE trending fault zones in the SCB, among which the Shaowu-Heyuan-Yangjiang Fault is one of the major fault zones (Figure 1). A large silicified quartz reef (up to 40 km of length and tens of meters thick) has developed along the Heyuan part of the fault zone and can be seen outcropping locally at several sites and visible in satellite imagery. The quartz reef is encased by a top phyllonitic seal and a bottom mylonitic zone (Tannock et al., 2020a). Another distinctive characteristic is that an abundance of hot springs are distributed along the Heyuan part of the fault zone (Tannock et al., 2020b).

Following the inferred slab roll-back in the Late Cretaceous, the SCB has transformed from an active margin to a passive continental margin. Continent rifting, break up and seafloor spreading occurred at the Andean-type margin along with the formation of the SCS basin during the early and middle Cenozoic (Taylor and Hayes, 1983; Wang et al., 2019). The relatively young continental lithosphere underwent extensive rifting from ~45 Ma. At ~33 Ma, continental breakup occurred in the northeast and led to the formation of the east sub-basin (ESB). Then, the spread center jumped to the south at around 25.5 Ma and the opening of the northwest sub-basin (NWSB) stopped. The spreading kept propagating southwestwards, leading to the formation of the southwest sub-basin (SWSB). In the middle Miocene (15 Ma), the seafloor spreading ceased (Franke, 2013; Savva et al., 2014; Li et al., 2018). The diachronous seafloor spreading from east to west in the Oligocene and Miocene results in the present-day V-shaped morphology of the SCS (Pichot et al., 2014) (Figure 1).

Due to the multiphase rifting and diachronous seafloor spreading, the northern SCS margin had experienced extreme crustal thinning (Yan et al., 2001; Savva et al., 2014; Lester et al., 2014). Significant along-strike variations in morphology, crustal structure and structural styles have been revealed by geophysical studies (Franke, 2013; Bai et al., 2019; Zhao et al., 2016; Yang et al., 2018). The northeast segment has a rugged topography with a seafloor characterized by local reliefs, and the northwest segment is characterized by a gentle morphology with a slightly dipping slope (Zhao et al., 2020). The east part of the SCS northern margin exhibits 400 km of extended crust, while the west part shows 800 km of extended continental crust (Hayes and Nissen, 2005; Pichot et al., 2014).

Abrupt thinning of continental crust in front of the continent–ocean transition zone (COT) and a narrow COT have been observed in the western segment of the SCS. In contrast, over the eastern segment, the continental crust thins gently and forms a relatively wide COT (Pichot et al., 2014). To explain this lateral variability, different extensional models have been proposed, such as polyphase faulting, sequential faulting and depth-dependent stretching (Clift et al., 2002; Huisman and Beaumont, 2014; Pichot et al., 2014; Zhao et al., 2018). Such variability may also be attributed to the heterogeneous crust of the SCB because of its extremely complex evolution. However, both the heterogeneous nature of the SCB and its relationship with the extensional variability along-strike the northern SCS margin have not been well documented.

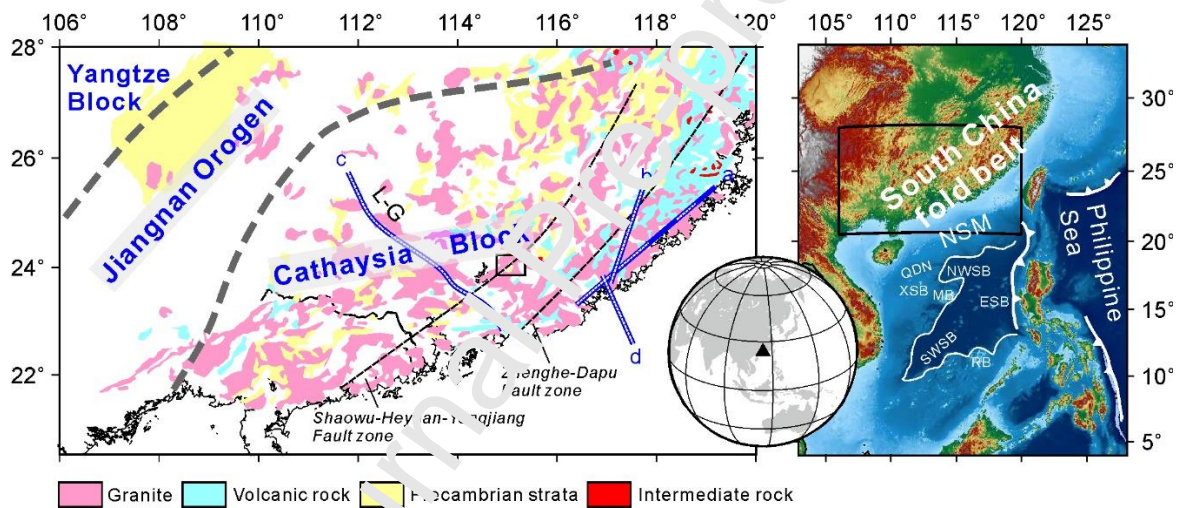


Figure 1 | General tectonic framework of the study area and its surrounding regions. Left panel: Gray thick dashed lines denote the borders of the Yangtze and the Cathaysia block. Black thin dashed lines indicate fault zones. Blue straight lines represent wide-angle deep seismic profiles in the study area with the extent of the LVLs indicated by white dashed lines. a. *Liao et al.*, 1988; b. *Xiong et al.*, 1991; c. *Yin et al.*, 1999; *Zhang and Wang*, 2007; *Zhao et al.*, 2013; d. *Zhao et al.*, 2004. Black box indicates the location of the giant quartz reef (modified after *Guo et al.*, 2019). Right panel: Tectonics of the surrounding region. NSM – northern SCS margin; ESB – east sub-basin; NWSB – northwest sub-basin; SWSB – southwest sub-basin; QDN – Qiongdongnan basin; XSB – Xisha block; MB – Macclesfield Bank; RB – Reed Bank.

3 Data and methods

3.1 Seismic data

This study used three-component waveforms recorded by 67 broadband seismic stations (Figures 1

and Figure 2) from 2012 to 2015. These permanent stations are part of the Guangdong Digital Seismograph Network (<http://www.gddzj.gov.cn/>) and China Earthquake Network Center (<https://www.cenc.ac.cn/>). With an average spacing of about 50 km, station distribution in the coastal area is deployed denser than in the north (Figure 2). Almost all stations are located in the Cathaysia block and only a few are located in the Jiangnan orogen (Figure 1). At each station, we selected teleseismic events from the International Seismological Center (ISC) catalog with magnitude $M_w > 5.5$ occurring at an epicentral distance between 30° and 90° . Our final data set contains 278 events for receiver function calculation (Figure 3).

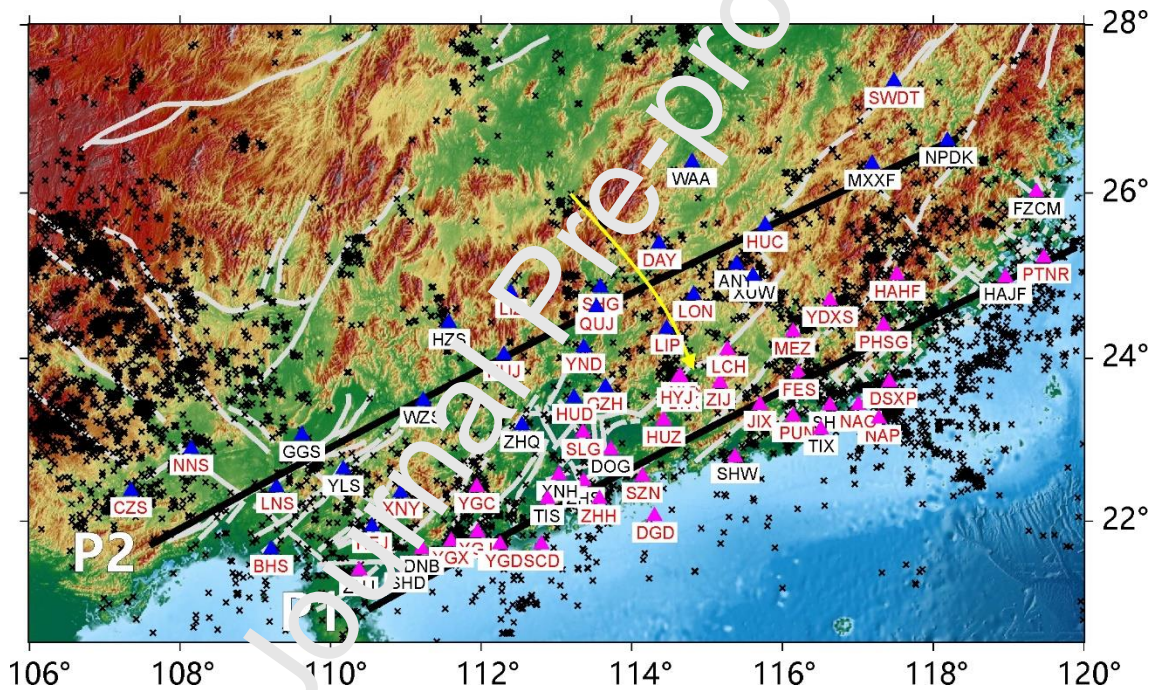


Figure 2 | Map of seismic stations (triangles) used in the analysis. Magenta triangles belong to section P1 and blue belong to P2. Gray lines mark the faults. Black crosses represent earthquakes (up to ML 5.2) in the past ten years provided by China Earthquake Data Center (<http://data.earthquake.cn/>). The yellow arrow point to the location of the giant quartz reef. Stations with red names show direct evidence for a mid-crustal LVL.

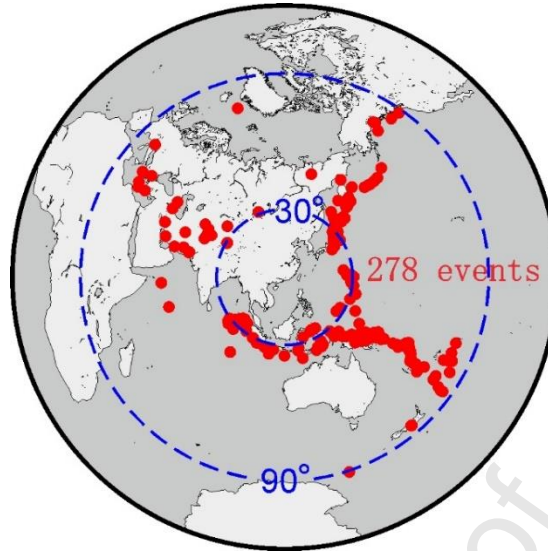


Figure 3 | Distribution of 278 teleseismic events (red dots) used in this study. Blue dashed lines indicate 30° and 90° epicentral distances from the center of the study area.

3.2 P-to-S receiver function

We use the receiver function technique to image intra-crustal LVLs. By deconvolving the vertical from the horizontal components, we remove the source time function, the possible source side effects and deep-Earth propagation effects and isolate the P-to-S conversions generated at velocity discontinuities beneath stations. We used the classical time-domain iterative deconvolution method (Ligorria and Ammon, 1999) to calculate P-to-S receiver functions. Before calculation, we first cut the teleseismic signals 30 s before and 120 s after the arrival time of the direct P phase based on the 1-D IASPEI91 velocity model (Kennett and Engdahl, 1991). To ensure the data set quality, we applied a semi-automatic quality control on the filtered original vertical-north-east (Z-N-E) waveforms following the method proposed by Hetenyi et al. (2015, 2018). 11'370 high-quality traces were selected from total 16'438 traces. We then rotated the Z-N-E components to a vertical-radial-transverse system (Z-R-T) based on the event back-azimuth. We downsampled the records at 20 Hz, removed the mean, applied a taper Hanning and band-pass filter at 0.2–1 Hz before RF calculation. After 150 iterations of the iterative deconvolution algorithm, the final radial and transverse RFs were obtained by a convolution of Gaussian pulse width corresponding to the signal's highest frequency. Assuming a crustal shear wave velocity of 3.6 km/s, the corresponding

wavelength is 3.6 km at 1 Hz. Based on the minimum resolvable length scale of $\lambda/4$, the layer thickness larger than ~ 0.9 km is resolvable. An example of radial RFs of station HUI is shown in Figure 4 and individual RFs at all stations can be found in Supporting Figure S1.

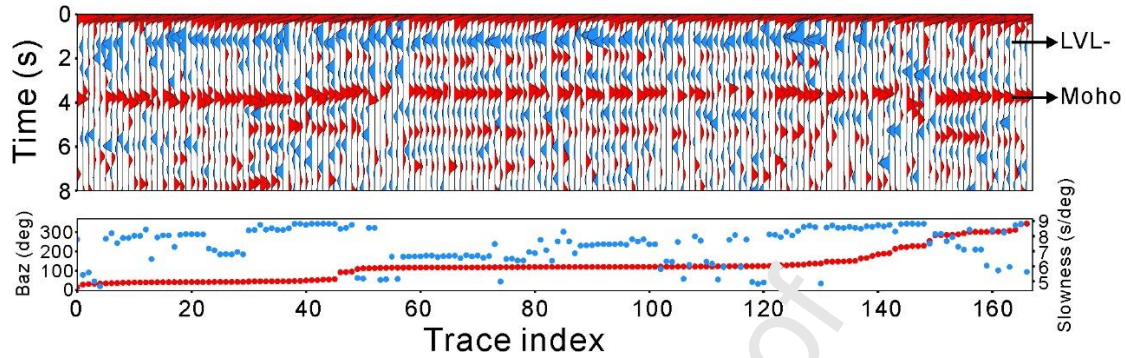


Figure 4 | An example of radial receiver functions of station HUI arranged as a function of back-azimuth using the time-domain iterative deconvolution in the frequency band of 0.2–1 Hz. The Moho and top of the LVL (LVL-) are labeled.

3.3 Common conversion point migration

We used the pre-stack migration method to map seismic discontinuities. Pre-stack migration allows the RF amplitudes to be mapped at the positions of P-to-S conversion along the ray path. Technically, we performed the time-to-depth migration using the widely adopted common conversion point (CCP) approach (Zhu, 2000). We first chose two parallel sections, P1 and P2, according to the station distribution. Then we projected sections onto the sections (95 km on both sides of P1, magenta triangles in Figure 2; 125 km on both sides of P2, blue triangles in Figure 2). Along the sections, the average station interval is 26 km for P1 and 40 km for P2 (Figures 5A and 6A). Given the nature of a relatively flat Moho and no strongly spatial variations in seismic velocity in the Cathaysia block (Zhou et al., 2012; He et al., 2013; Guo et al., 2019), we employed a 1D P and S wave velocity model derived from the deep seismic profile L-G (Figure 1) (Zhang and Zhao, 2007; Zhao et al., 2013) for time-to-depth conversion (Table 1). To further improve the imaging, a 3D velocity model should be used in the future to take into account small-scale crustal velocity heterogeneities. We projected RF amplitudes onto the profiles with a depth interval of 1 km and a horizontal bin of 15 km, which is close to the Fresnel zone radius at the Moho. Later, images are horizontally smoothed with a 40 km Gaussian filter. The migration takes the station elevation into account.

Table 1. 1-D Velocity Model used for time-to-depth migration (Zhang and Zhao, 2007; Zhao et al., 2013). The V_p/V_s ratio considered in the three layers are 1.73, 1.71 and 1.74 respectively.

	0-10km	10-20km	20-35km
P (km/s)	5.92	6.07	6.65
S (km/s)	3.42	3.55	3.82

4 Results

The Moho is visible as strong, positive interface (warm color) in Figures 5 and 6, in a depth range of 25–34 km. We picked the Moho (the maximum amplitude at depth beneath each station) to map the Moho geometry in 3D, it is shallower in the western part (25–27 km) and deeper in the east (28–34 km) (Figure 7B). The shallowest Moho appears at around 110°E, while the deepest Moho is located between 110°–120°E. A slight decrease of Moho depth from continental interior to the coast can be observed, by 2–3 km. The depth variation in the Moho is consistent with previous results (26–34 km) obtained with a single-station grid search technique (Zhu and Kanamori, 2000; Chevrot and van der Hilst, 2000; He et al., 2013; Xia et al., 2015; Guo et al., 2019). The 1D migration model has small influences on the determination of the Moho depth, probably because of the nature of a relatively flat Moho and no strongly lateral variations in speed velocity in the study area (Zhou et al., 2012; He et al., 2013; Guo et al., 2019). This gives support to the credibility of the intra-crustal interfaces as described below.

Besides the Moho conversion, we can observe a series of negative pulses (shown in blue) distributed between 1–2 s in Figures 5B and 6B, representing a sharp negative velocity gradient with depth. Since the study area is largely covered by igneous rocks (Figure 1), it is unlikely that the negative conversion is influenced by a shallow sedimentary layer. In addition, we don't observe strong positive conversions before the negative arrivals (Figure 4 and Figure S1). In the CCP migrated images, these negative polarity interfaces (cold color) are distributed at 9–16 km depth (Figures 5D and 6D), and with amplitudes smaller compared to that of the Moho. Along P1, the negative polarity interfaces vary in a depth range of 12–16 km and rather strong amplitudes are visible between 600–800 km distance (Figures 5D). Other negative amplitude patches in the crust (e.g. 5 km depth at 300–400 km distance, and lower-crustal variable depth at 600–800 km) have smaller amplitudes and we consider them as secondary with respect to the main mid-crustal LVL. The CCP image of P2

(Figures 6D) shows two groups of blue patches along 100–200 km and 500–800 km, lying relatively flat at around 10 km depth. We picked the depths of these continuous negative interfaces at the local minima beneath each station (crosses in Figures 5D and 6D) and plotted them in map view (Figure 7A). We can see that the negative polarity interfaces appear broadly in the eastern Cathaysia block, with depths shallower in the northwest (~10 km) and deeper in the southeast (~12–16 km). The deepest negative interfaces are located between longitude 111°–114°E. The corresponding amplitude map of the negative interfaces shows variable values between -0.03 to -0.1. An evidential trend is that the amplitudes generally strengthen eastwards, with the strongest amplitude appearing at around longitude 116°E (Figure 7C).

P-to-S receiver function phases can be influenced by the presence of azimuthal anisotropy or a significant dip on the discontinuity, both of which are not unexpected in the highly complex SCB with a history of multiple collisional cycles. A dipping layer will generate a zero-lag arrival on the transverse RFs that is not observed in the anisotropic case. In this study, clear zero-lag arrivals of the transverse components can be observed at station Σ U ω , JIX, LIP and PHSG (Figure S1). However, it is difficult to assess which dipping interface of these zero-lag signals come from. The effects of a possible anisotropic layer are more complicated. For most of the stations, energy on the transverse RFs appears in the range of 1–2 s is small compared to that on the corresponding radial RFs, which indicates that anisotropy is not the dominant source of signal in this study. The above analysis points to largely isotropic velocity decrease at horizontal boundaries.

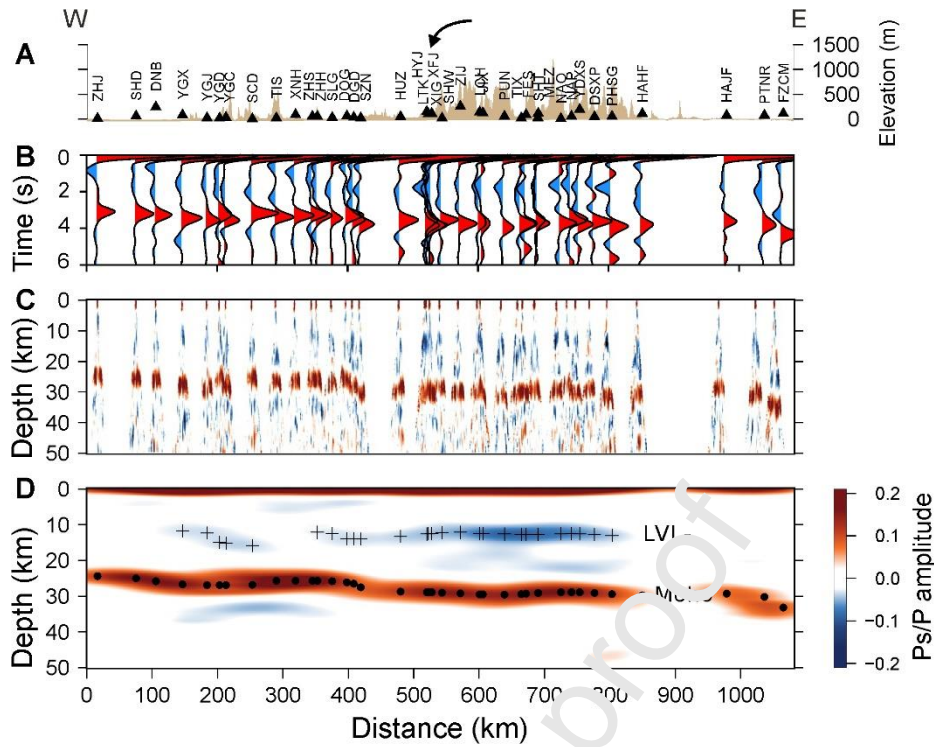


Figure 5 | Receiver function images of section P1. From top to bottom panels: **A.** Topographic profile, with triangles indicating station locations. The black arrow indicates the location of a giant quartz reef. **B.** Single-station stacked radial receiver function traces. Red pulses correspond to positive velocity gradients; blue pulses correspond to negative velocity gradients with depth. **C.** Individual receiver function traces plotted along profile representing raypaths of individual phase arrivals. **D.** Common conversion point migrated image with amplitudes indicated by color bar at right. Black dots represent the estimated Moho depth and crosses indicate the inferred top interfaces of the LVLs.

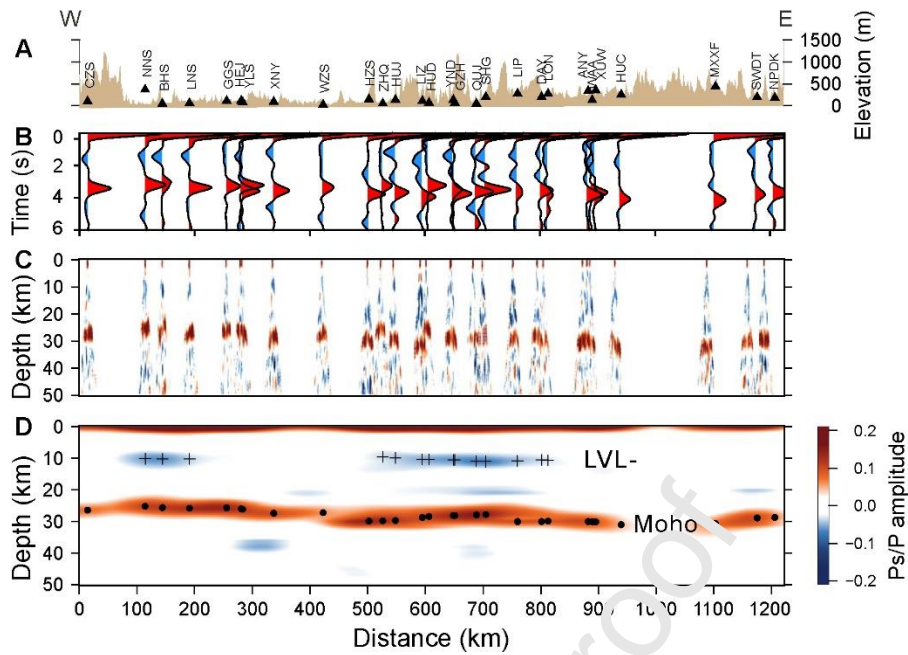


Figure 6 | Receiver function images of section P2. Same panels as in Figure 3.

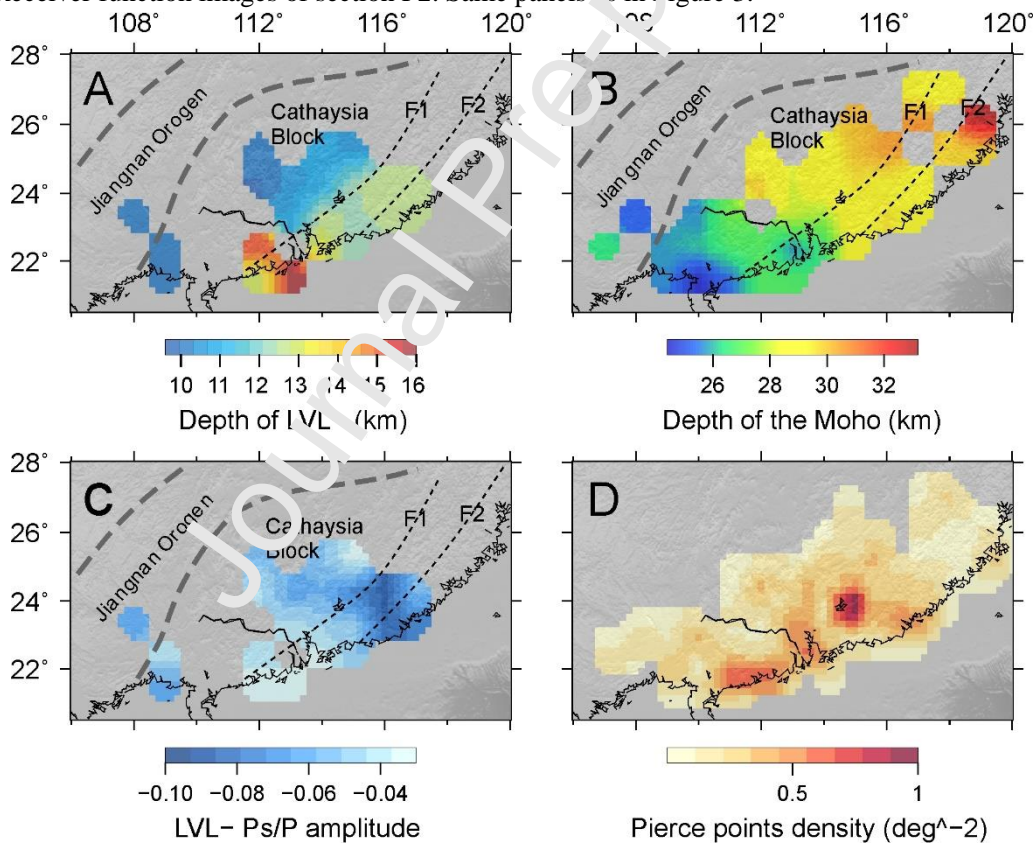


Figure 7 | **A.** Topography of the LVL-. LVL- – the top of the low-velocity layer. Gray thick dashed lines denote the borders of the Yangtze and the Cathaysia block. Black thin dashed lines indicate the fault zones. F1: Shaowu-Heyuan-Yangjiang Fault zone. F2: Zhenghe-Dapu Fault zone. **B.** Topography of the Moho. **C.** Amplitude map of the LVL-. **D.** Normalized RF ray piercing points density map.

5 Discussion

5.1 Low-velocity layer: nature and origin

Based on previous studies (Liao et al., 1988; Xiong et al., 1991; Yin et al., 1999; Zhang and Wang, 2007; Zhao et al., 2013), we interpret the negative velocity gradients in the mid-crust of our CCP images as the top interfaces of the low-velocity layer. They show depth variations in good agreement with different geophysical sounding velocity models, although the top of the LVLs from former results are locally deeper (gray dashed lines in Figure 8a). This may reflect differences in the ability of active- versus passive-source imaging techniques to characterize structure in the intra-crust. We couldn't present the thickness distribution of the LVLs, because the bottom interfaces of the LVLs are not observed, a phenomenon that has also been reported in some of the deep seismic profiles. For example, Zhao et al. (2004) didn't find the reflected phases from the bottom of the LVLs (profile d in Figure 1). The reflected phases are not clear in Liao et al. (1988)'s profiles (profile a in Figure 1). The most likely reason is a spatially broad (~10 km) velocity gradient with depth, not sensed by receiver functions due to its vertical extent (a dipping interface or an anisotropic layer is not a dominant feature in this study as discussed above). The absolute amplitudes of the negative interfaces in our RF profiles are small compared to that of the Moho. This may indicate limited velocity/impedance contrast between LVLs and upper layers. In fact, the velocity profile of L-G shows that the P-wave velocity of the LVLs is 5.8 km/s, underlying an upper layer with velocity of 6.2-6.3 km/s (Zhang and Zhao, 2007), and 3.5 km/s underlying 3.6-3.65 km/s for S-wave velocity (Zhao et al., 2013), thus leading to a V_p/V_s ratio of around 1.66 of the LVLs. The only common mineral with such a very low V_p/V_s ratio is quartz (Christensen, 1996), which suggests that the LVLs have high quartz concentrations and may be related to fluids.

Most of the previous workers attributed the LVLs in our study area to partial melting within the mid-crust. However, the relatively low V_p/V_s ratio (~1.66) does not support the presence of partial melt in the crust, as large amounts of partial melt would increase V_p/V_s (Watanabe, 1993). Besides, the last peak age of magmatism in south China is around 93 Ma (Wang et al., 2013). It is unlikely that partially melt bodies are still preserved after such a long period of cooling. Another common interpretation of the LVLs in the orogenic zone is the remnant of crustal materials after subduction or collision, such as accretionary complexes or felsic upper-middle crust. Yet, such remnants often

show dip from mid- to lower-crust and mostly in the lower-crust (Zheng et al., 2009; Smit et al., 2016) while the LVLs in our study area are relatively flat within the mid-crust. Therefore, we favor the interpretation of LVLs related to fluids from dehydration of the subducting slab and trapped in the mid-crust (Figure 8b). In south China, due to the flat-slab subduction of the paleo-Pacific plate, a ~1300-km-wide orogenic belt was formed in the Triassic (Li and Li, 2007; Liu et al., 2017). During subduction, fluids produced by dehydration of the slab are expected to migrate into the mantle and upper plate by channelized flow or along grain boundaries (Jamtveit et al., 2016). Such transportation allows fluids to migrate at relatively large distances in a geologically rapid way and only a small volume of water can be absorbed by the mantle wedge (John et al., 2012; Wada et al., 2012; Jonas et al., 2014). It is possible that the additional fluids trapped in the mid-crust cause the observed reduction of seismic wave velocity (Figure 8b). Owing to its lower bulk modulus, fluids can reduce the compressional and shear velocity. Based on the model of Watanabe (1993) on granite, a V_p/V_s of 1.66 suggests a fluid fraction in the range of ~15 percent. Intra-crustal LVLs have long been found in western North and South America, where several low-angle and flat-slab subduction occur, and these LVLs are thought to be fluid related (Yuan et al., 2001; Beck and Zandt, 2002; Jödicke et al., 2006; Wannamaker et al., 2014; Araya Vargas et al., 2019). Free water generated by dehydration of the downgoing oceanic plate can be trapped in the mid- and lower crust below an impermeable layer formed through mineral precipitation when temperature conditions are met (Jones, 1987). Very low permeability, of less than 10^{-20} m², allows fluids to reside for hundreds of millions of years (Hyndman 1988).

Rising fluids released from the subducted oceanic slab are thought to be silica saturated and the deposition of silica with decreasing temperature and pressure is expected to form quartz (Hyndman et al., 2015), some of which is presently exposed as quartz veins, such as in New Zealand (Breeding and Ague, 2002) and Alaska (Fisher and Brantley, 2014). In south China, a more than 40-km-long and 75-m-width giant quartz reef is exhumed where stations LTK, XFJ, HYJ and XIG are located (Figures 1, 2, 5 and 8c). Microstructural analyses revealed that this quartz reef was formed at mid-crustal conditions, for which significant volumes of metamorphic and meteoric fluids were required (Tannock et al., 2020a). The changes in morphology and grain size are controlled by the transformation of stress regime since the Mesozoic, and the present-day hot springs are still fed by

deep fluid sources via a fracture network (Tannock et al., 2020b).

We acknowledge that there may be other interpretations. For example, a sub-horizontal or shallowly dipping crustal detachment extending over hundreds of kilometers cannot be ruled out. However, if there is such an architecture due to the paleo-Pacific plate subducting beneath the Cathaysia block, the dipping would be northwestwards, opposite to our findings. Our 1D velocity model used in the migration may lead to slightly distorted dip estimates. However, observations from active source imaging revealed an even more flat LVL (Figure 8a) (Liao et al., 1988; Xiong et al., 1991; Yin et al., 1999; Zhao et al., 2004; Zhang and Wang, 2007; Zhao et al., 2013)

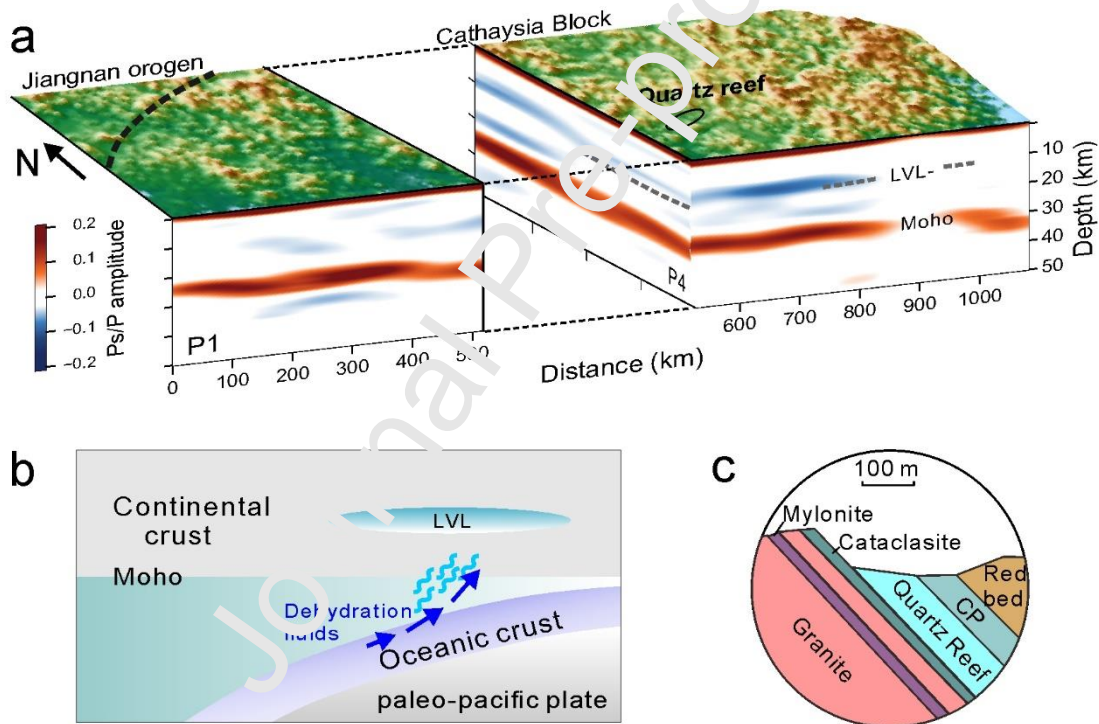


Figure 8 | (a) CCP image of the crustal structure along profile P1 (Figure 2) and P4 (Figure 9). Gray lines indicate the top of the LVLs by former studies (Liao et al., 1988; Zhang and Wang, 2007; Zhao et al., 2013). The Quartz reef is marked by an oval. (b) Interpretative diagram showing the migration of dehydration fluids coming from the Paleo-pacific slab and the accumulation of fluids in the mid-crust. (c) Cross-sectional view of the giant quartz reef. CP – Cataclasite-Phyllonite. (modified from Tannock et al., 2020a).

5.2 Spatial variation of the Low-velocity layer

The presence of the mid-crustal LVLs shows a longitudinal difference. That is, the LVLs mainly

distributed in the eastern Cathaysia block spanning over 500 km, with increasing strength eastwards within the mapped volume (Figure 7C). Also, the Moho is about 3–4 km deeper in the eastern Cathaysia block than in the west. The Moho depth exhibits a slight decrease towards the coast. On the contrary, the depth of the LVLs becomes shallower towards the continental interior (Figure 7). Such distribution may be determined by inherited conditions: 1) the lateral variations in the degree of hydration of the incoming plate, 2) variations in permeability structure of the subduction oceanic plate, and 3) variations in permeability of the upper plate. Heterogeneity of the incoming plate hydration are controlled by variations in density and the maximum fault throw (vertical component of fault displacement) of bending-related faults (Boneh et al., 2019), and the permeability structure of the downgoing slab ultimately determines the release of fluids (Delph et al., 2018). The difference in rock porosity or permeability of the upper plate controlled by fluid and rock composition can also lead to the observed lateral variation of the LVLs (Hyndman 1988; Araya Vargas et al., 2019), even though we cannot give direct evidence.

The depth variation of the LVLs in this study is compared to these reported in western North and South America. The LVL in the northern Cascadia subduction zone, labeled as ‘E’ layer, shows landwards dipping following the isotherm temperature of 400-500°C (Hyndman, 1988). However, most of the other LVLs exhibit irregular variations in depth (Beck and Zandt, 2002; Jödicke et al., 2006), similar to our results. To be noticed, the observed LVLs may have different causes because clear depth variation of the LVLs can be seen in Figure 7A and Figure 9C. The amplitude variation of the LVL- is independent of RF ray sampling as shown by both the profile (Figure 5 and 6) and map (Figure 7) views. Thus, it may be a reflection of water content, with larger values concentrated in the east. Such variation may be also determined by the inherited conditions as discussed above. The spatial presence, depth variation and the amplitude variation of the LVLs can be reworked by subsequent processes, such as asthenosphere upwelling caused by slab break-off and full-scale foundering in the continental interior, as well as slab roll-back along the southeastern coast (Li and Li, 2007; Li et al., 2007). The additional reheating or re-dehydrating by these post-orogenesis mechanisms is expected to alter the LVLs following an NW-SE orientation, however, we didn’t find a very clear trend.

5.3 Implications for continental rift

A fluid-filled layer will inevitably have a large influence on crustal rheology. Laboratory experiments showed that even small concentrations (of a few tens of parts per million) of water contained in hydrous minerals can decrease strength dramatically (Mackwell et al., 1998). The spatial distribution of the LVLs emphasizes the lateral difference in rheological structure in the Cathaysia block (Figure 7 and 9), with the eastern segment expected to be less viscous and mechanically weaker. In a fault zone near station NAP (Figure 2), swarm-type seismicity has been observed and mainly occurs in a mid-crustal low-velocity zone (LVZ). The LVZ is relatively continuous at about 13–15 km depth (Xia et al., 2020). High pore pressure due to the trapped fluids or fluids induced strain localization (Getsinger et al., 2013) may be responsible for this mid-crustal seismicity layer. In the late Mesozoic, the SCB has transformed from an active margin to a passive continental margin. Continent rifting, break up and seafloor spreading occurred at the Andean-type margin along with the formation of the SCS basin. Situated in the transition between the tectonically complex SCB and the newly formed SCS (Figure 1), the coastal area may largely record the pre-rift or early-stage rift structures inherited from subduction and orogenesis (for instance, the LVLs), shortly before the onset of continental failure and seafloor spreading. To the south, longitudinal contrast in crustal structures, stretching and faulting along-strike the northern SCS rifted margin have been reported by geological and geophysical observations (Bai et al., 2015, Zhao et al., 2020). While the east part of the northern SCS margin (NSM) exhibits relatively wide necking or distal domain, the west part shows a wide proximal domain and a narrow necking zone (Yang et al., 2018), which indicates a reducing degree of crustal stretching from east to west on the lower continental slope (Figure 9a). The lateral variation of the presence of the LVLs is spatially consistent with the along-strike variation in crustal stretching along the NSM, suggesting that they may be related.

To connect observations onshore and offshore, we chose three seismic profiles including OBS200 (Wang et al., 2006), OBS1993 (Yan et al., 2001) and ESP-W1985 (Nissen et al., 1995), from eastern, central and western SCS northern margin; correspondingly, three RF profiles were produced from our results as the extensions of the above offshore profiles, namely P3, P4 and P5 (Figure 9a). Over the eastern segment, a clear mid-crustal LVL onshore and a wide COT offshore are shown (Figure 9b and 9e). While in the western segment, LVL is invisible and a COT-like thinned crust is narrow (Figure 9c and 9f). The central part exhibits transitional characteristics (Figure 9d and 9g). According

to the numerical analysis by Li et al. (2019), the rheologically weak LVLs in the mid-crust could control the width of the highly thinned crust (thickness smaller than 15 km) and the crustal thermal distribution by accommodating deformation during extension. They therefore proposed that thicker LVLs result in wider range of ultra-thinned crust in the eastern NSM, while thinner LVLs are responsible for narrower range of ultra-thinned crust in the western NSM. Here, we supplement observations and explanations on the variability of LVL signal strength. The west segment of the NSM might experience more complex evolution because of the limited distribution of LVLs, for instance, the unresolved cessation of seafloor spreading in the northwest sub-basin (NWSB), the failed hyper-extension rift in the Qiongdongnan basin (QDN), the jump of the spreading ridge from the NWSB to the southwest sub-basin (SWSB) (Li et al., 2018; Zhao et al., 2018). The presence of several rigid blocks in the western SCS, e.g. the Xisha block (XSB), Macclesfield Bank (MB) (Figure 9a), which are inherited from the SCB (Yan et al., 2010) and deformed weakly during the rifting phase (Ding and Li, 2016; Lü et al., 2017), may be the most direct evidence. Actually, the fact that crust in the western NSM is more rigid than that in the east has been noticed long ago (Clift et al., 2002) and such phenomenon is suspected to be partly caused by the heterogenous nature of the SCB crust (Pichot et al., 2014). Here, we provide a direct observation of crustal heterogeneity from the perspective of crustal hydration, and emphasize the importance of inheritance in controlling the along-strike variations of rifting styles in the northern SCS margin. To be noticed, there are other hypotheses explaining this along-strike variation. For example, the V-shape geometry of propagating rift systems may also be responsible for such variation.

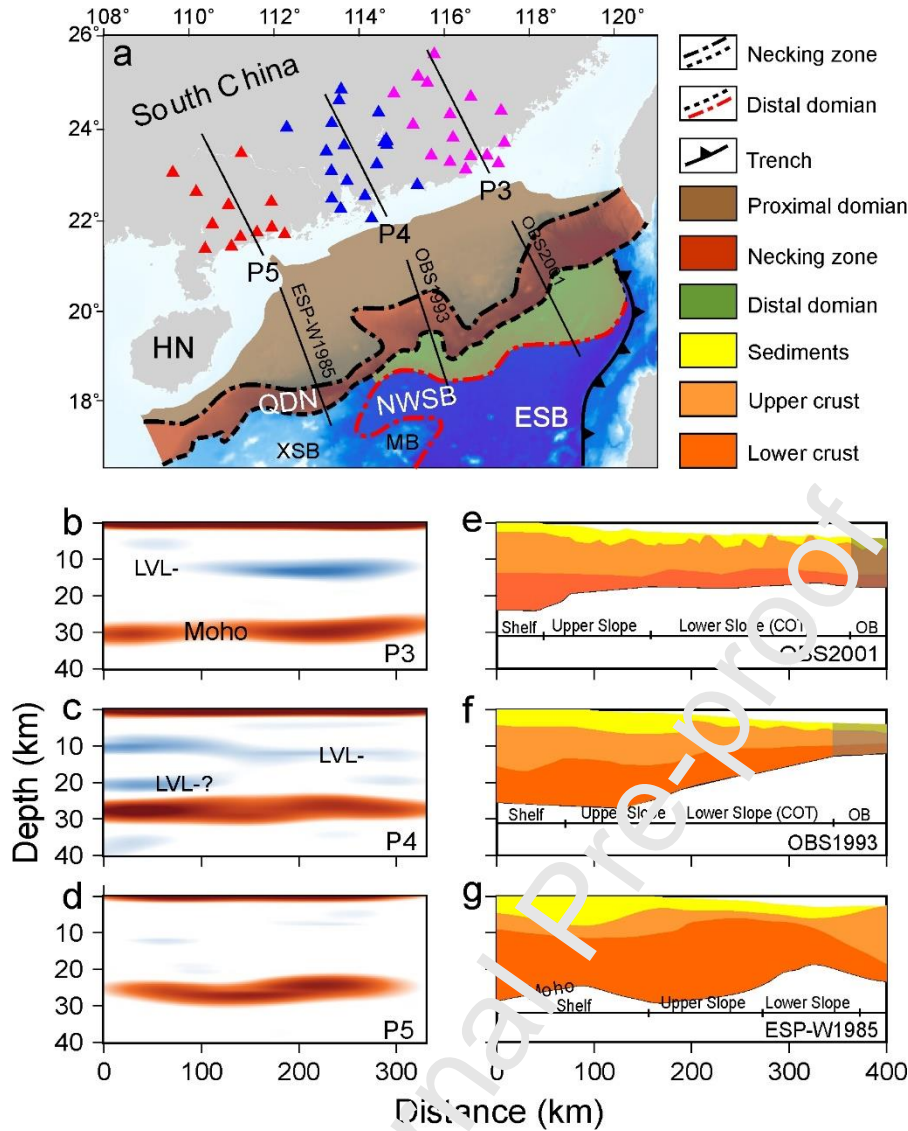


Figure 9 | Comparison of onshore and offshore crustal structures. (a) Onshore and offshore sections represented by black lines. Magenta, blue and red triangles indicate seismic stations for section P3, P4 and P5. Major extensional domains are shown in the northern SCS margin according to (Yang et al., 2018). (b - d) CCP images of section P3, P4 and P5. (e - g) Velocity structures along profile OBS2001 (Wang et al., 2006); profile OBS1993 (Yan et al., 2001) and transect ESP-W (Nissen et al., 1995). HN – Hainan Island; ESB – east sub-basin; NWSB – northwest sub-basin; QDN – Qiongdongnan basin; XSB – Xisha block; MB – Macclesfield Bank; COT – continent-ocean transition; OB – oceanic basin.

6 Conclusions

Using over 10'000 receiver functions, we imaged the intra-crustal discontinuities beneath the coastal area of the northern South China Sea with the pre-stack CCP migration method. We found negative polarity interfaces broadly distributed in the eastern Cathaysia block, with depth varying from 9-16 km, inferred as the top of low-velocity layers. We interpreted these LVLs as fluids released by dehydration of the slab during the flat subduction of the paleo-Pacific plate in the Mesozoic, and

trapped in the mid-crust by impermeable layers, thus allowing fluids to reside for over hundred million years. Such structural inheritance, acting as weakened domains, might facilitate development of lateral heterogeneity of crustal rheology, and, subsequently, cause or influence significant variations in crustal structure along strike the northern SCS rifted margin.

Acknowledgements

We thank the Data Management Centre of China National Seismic Network at Institute of Geophysics, China Earthquake Administration (doi:10.11998/SeisDmc/SN, <http://www.seisdmc.ac.cn>) for providing waveform data for this study. We thank Lisa Tannock for sharing their unpublished manuscript. We thank Xusong Yang and Shiba Subedi for their technical help. This work is supported by the National Natural Science Foundation of China (Grant No. U1701641), Key Special Project for Introduced Talents Team of Southern Marine Science and Engineering Guangdong Laboratory (Guangzhou) (CML2019ZD0204), K.C. Wong Education Foundation (GJTD-2018-13), the Research Foundation of Guangdong Province of China (2019BT2H594), the Rising Star Foundation of the South China Sea Institute of Oceanology (NHXX2017DZ0101). The authors gratefully acknowledge financial support from China Scholarship Council (NO. 201804910670).

References

- Araya Vargas, J., Meqbel, N. M., Ritter, O., Brasse, H., Weckmann, U., Yáñez, G., & Godoy, B. (2019). Fluid Distribution in the Central Andes Subduction Zone Imaged With Magnetotellurics. *Journal of Geophysical Research: Solid Earth*, *124*(4), 4017-4034.
- Bai, Y., Wu, S., Liu, Z., Müller, F. D., Williams, S. E., Zahirovic, S., & Dong, D. (2015). Full-fit reconstruction of the South China Sea conjugate margins. *Tectonophysics*, *661*, 121-135.
- Bai, Y., Dong, D., Brune, S., Wu, S., & Wang, Z. (2019). Crustal stretching style variations in the northern margin of the South China Sea. *Tectonophysics*, *751*, 1-12.
- Bao, X., Sun, X., Xu, M., Eaton, D. W., Song, X., Wang, L., ... & Huang, Z. (2015). Two crustal low-velocity channels beneath SE Tibet revealed by joint inversion of Rayleigh wave dispersion and receiver functions. *Earth and Planetary Science Letters*, *415*, 16-24.
- Beaumont, C., Jamieson, R. A., Nguyen, M. H., & Lee, B. (2001). Himalayan tectonics explained by extrusion of a low-viscosity crustal channel coupled to focused surface denudation. *Nature*, *414*(6865), 738.
- Beck, S. L., & Zandt, G. (2002). The nature of orogenic crust in the central Andes. *Journal of Geophysical Research: Solid Earth*, *107*(B10), ESE-7.
- Boneh, Y., Schottenfels, E., Kwong, K., van Zelst, I., Tong, X., Eimer, M., ... & Billen, M. (2019). Intermediate-

- depth earthquakes controlled by incoming plate hydration along bending-related faults. *Geophysical Research Letters*, 46(7), 3688-3697.
- Breeding, C. M., & Ague, J. J. (2002). Slab-derived fluids and quartz-vein formation in an accretionary prism, Otago Schist, New Zealand. *Geology*, 30(6), 499-502.
- Caldwell, W. B., Klemperer, S. L., Lawrence, J. F., & Rai, S. S. (2013). Characterizing the Main Himalayan Thrust in the Garhwal Himalaya, India with receiver function CCP stacking. *Earth and Planetary Science Letters*, 367, 15-27.
- Chevrot, S., & van der Hilst, R. D. (2000). The Poisson ratio of the Australian crust: geological and geophysical implications. *Earth and Planetary Science Letters*, 183(1-2), 121-132.
- Christensen, N. I. (1996). Poisson's ratio and crustal seismology. *Journal of Geophysical Research: Solid Earth*, 101(B2), 3139-3156.
- Clift, P., Lin, J., & Barckhausen, U. (2002). Evidence of low flexural rigidity and low viscosity lower continental crust during continental break-up in the South China Sea. *Marine and Petroleum geology*, 19(8), 951-970.
- Delph, J. R., Levander, A., & Niu, F. (2018). Fluid controls on the heterogeneous seismic characteristics of the Cascadia margin. *Geophysical Research Letters*, 45(20), 11-021.
- Deng, Y., Li, J., Peng, T., Ma, Q., Song, X., Sun, X., ... & Fan, W. (2019). Lithospheric structure in the Cathaysia block (South China) and its implication for the Late Mesozoic magmatism. *Physics of the Earth and Planetary Interiors*, 291, 24-34.
- Ding, W., & Li, J. (2016). Conjugate margin pattern of the Southwest Sub-basin, South China Sea: insights from deformation structures in the continent-ocean transition zone. *Geological Journal*, 51, 524-534.
- Festa, A., Balestro, G., Borghi, A., De Caroli, S., & Succo, A. (2020). The role of structural inheritance in continental break-up and exhumation of Alpine Tethyan mantle (Canavese Zone, Western Alps). *Geoscience Frontiers*, 11(1), 167-188.
- Franke, D. (2013). Rifting, lithosphere breakup and volcanism: Comparison of magma-poor and volcanic rifted margins. *Marine and Petroleum geology*, 43, 63-87.
- Fisher, D. M., & Brantley, S. L. (2012). The role of silica redistribution in the evolution of slip instabilities along subduction interfaces: Constraints from the Kodiak accretionary complex, Alaska. *Journal of Structural Geology*, 69, 395-414.
- Getsinger, A. J., Hirth, G., Stünitz, H., & Goergen, E. T. (2013). Influence of water on rheology and strain localization in the lower continental crust. *Geochemistry, Geophysics, Geosystems*, 14(7), 2247-2264.
- Guo, L., Gao, R., Shi, L., Huang, Z., & Ma, Y. (2019). Crustal thickness and Poisson's ratios of South China revealed from joint inversion of receiver function and gravity data. *Earth and Planetary Science Letters*, 510, 142-152.
- Hayes, D. E., & Nissen, S. S. (2005). The South China sea margins: Implications for rifting contrasts. *Earth and Planetary Science Letters*, 237(3-4), 601-616.
- He, C., Dong, S., Santosh, M., & Chen, X. (2013). Seismic evidence for a geosuture between the Yangtze and Cathaysia Blocks, South China. *Scientific reports*, 3, 2200.
- Hetényi, G., Plomerová, J., Bianchi, I., Exnerová, H. K., Bokelmann, G., Handy, M. R., ... & AlpArray-EASI Working Group. (2018). From mountain summits to roots: Crustal structure of the Eastern Alps and Bohemian Massif along longitude 13.3° E. *Tectonophysics*, 744, 239-255.

- Hetényi, G., Ren, Y., Dando, B., Stuart, G. W., Hegedűs, E., Kovács, A. C., & Houseman, G. A. (2015). Crustal structure of the Pannonian basin: the AlCaPa and Tisza Terrains and the Mid-Hungarian zone. *Tectonophysics*, *646*, 106-116.
- Hetényi, G., Vergne, J., Bollinger, L., & Cattin, R. (2011). Discontinuous low-velocity zones in southern Tibet question the viability of the channel flow model. *Geological Society, London, Special Publications*, *353*(1), 99-108.
- Hu, X. Y., Bi, G. X., Liu, J. T., Han, J. C., Cai, R. H., Peng, S. Xu, and S. J. Liu (2017), The Lithospheric Electrical Structure of JI'AN-FUZHOU Profile in the East Part of South China, *Chinese Journal of Geophysics*, *60*(5), 532-543.
- Huisman, R. S., & Beaumont, C. (2014). Rifted continental margins: The case for depth-dependent extension. *Earth and Planetary Science Letters*, *407*, 148-162.
- Hyndman, R. D., McCrory, P. A., Wech, A., Kao, H., & Ague, J. (2015). Cascadia subducting plate fluids channelled to fore-arc mantle corner: ETS and silica deposition. *Journal of Geophysical Research: Solid Earth*, *120*(6), 4344-4358.
- Hyndman, R. D. (1988). Dipping seismic reflectors, electrically conductive zones, and trapped water in the crust over a subducting plate. *Journal of Geophysical Research: Solid Earth*, *93*(B11), 13391-13405.
- Jamtveit, B., Austrheim, H., & Putnis, A. (2016) Disequilibrium metamorphism of stressed lithosphere. *Earth-Science Reviews*, *154*, 1-13.
- Jödicke, H., Jording, A., Ferrari, L., Arzate, J., Mezger, K. & Rüpke, L. (2006). Fluid release from the subducted Cocos plate and partial melting of the crust deduced from magnetotelluric studies in southern Mexico: Implications for the generation of volcanism and subduction dynamics. *Journal of Geophysical Research: Solid Earth*, *111*(B8).
- John, T., Gussone, N., Podladchikov, Y. Y., Babout, G. E., Dohmen, R., Halama, R., ... & Seitz, H. M. (2012). Volcanic arcs fed by rapid pulsed fluid flow through subducting slabs. *Nature Geoscience*, *5*(7), 489.
- Jonas, L., John, T., King, H. E., Geisler, T., & Putnis, A. (2014). The role of grain boundaries and transient porosity in rocks as fluid pathways for reaction front propagation. *Earth and Planetary Science Letters*, *386*, 64-74.
- Jones, A. G. (1987). MT and reflection: an essential combination. *Geophysical Journal International*, *89*(1), 7-18.
- Kennett, B. L. N., & Engdahl, E. R. (1991). Traveltimes for global earthquake location and phase identification. *Geophysical Journal International*, *105*(2), 429-465.
- Lester, R., Van Avendonk, H. J., McIntosh, K., Lavier, L., Liu, C. S., Wang, T. K., & Wu, F. (2014). Rifting and magmatism in the northeastern South China Sea from wide-angle tomography and seismic reflection imaging. *Journal of Geophysical Research: Solid Earth*, *119*(3), 2305-2323.
- Li, F., Sun, Z., Pang, X., Liao, J., Yang, H., Xie, H., ... & Zhao, Z. (2019). Low-viscosity crustal layer controls the crustal architecture and thermal distribution at hyper-extended margins: Modeling insight and application to the northern South China Sea margin. *Geochemistry, Geophysics, Geosystems*.
- Li, F., Sun, Z., & Yang, H. (2018). Possible spatial distribution of the Mesozoic volcanic arc in the present-day South China Sea continental margin and its tectonic implications. *Journal of Geophysical Research: Solid Earth*, *123*(8), 6215-6235.
- Li, X. H., Li, Z. X., Li, W. X., Liu, Y., Yuan, C., Wei, G., & Qi, C. (2007). U–Pb zircon, geochemical and Sr–Nd–Hf isotopic constraints on age and origin of Jurassic I- and A-type granites from central Guangdong, SE China: a

- major igneous event in response to foundering of a subducted flat-slab?. *Lithos*, 96(1-2), 186-204.
- Li, Z. X., & Li, X. H. (2007). Formation of the 1300-km-wide intracontinental orogen and postorogenic magmatic province in Mesozoic South China: a flat-slab subduction model. *Geology*, 35(2), 179-182.
- Li, Z. X., Li, X. H., Zhou, H., & Kinny, P. D. (2002). Grenvillian continental collision in south China: New SHRIMP U-Pb zircon results and implications for the configuration of Rodinia. *Geology*, 30(2), 163-166.
- Liao, Q. L., Z. M. Wang, P. L. Wang, Z. K. Yu, N. Y. Wu, and B. C. Liu (1988), Explosion seismic study of the crustal structure in Fuzhou-Quanzhou-Shantou region, *Chinese Journal of Geophysics (in Chinese with English abstract)*, 3, 270-280.
- Ligorria, J. P., & Ammon, C. J. (1999). Iterative deconvolution and receiver-function estimation. *Bulletin of the seismological Society of America*, 89(5), 1395-1400.
- Liu, X., Zhao, D., Li, S., & Wei, W. (2017). Age of the subducting Pacific slab beneath East Asia and its geodynamic implications. *Earth and Planetary Science Letters*, 464, 166-174.
- Long, M. D., Benoit, M. H., Aragon, J. C., & King, S. D. (2019). Seismic imaging of mid-crustal structure beneath central and eastern North America: Possibly the elusive Grenville deformation?. *Geology*, 47(4), 371-374.
- Lü, C., Hao, T., Lin, J., & Qiu, X. (2017). The role of rifting in the development of the continental margins of the southwest subbasin, South China Sea: Insights from an OBS experiment. *Marine Geophysical Research*, 38(1-2), 105-123.
- Mackwell, S. J., Zimmerman, M. E., & Kohlstedt, D. L. (1998). High-temperature deformation of dry diabase with application to tectonics on Venus. *Journal of Geophysical Research: Solid Earth*, 103(B1), 975-984.
- Manatschal, G., Lavier, L., & Chenin, P. (2015). The role of inheritance in structuring hyperextended rift systems: Some considerations based on observations and numerical modeling. *Gondwana Research*, 27(1), 140-164.
- Marzen, R. E., Shillington, D. J., Lizarralde, D., & Harder, S. H. (2019). Constraints on Appalachian Orogenesis and Continental Rifting in the Southeastern US from Wide-Angle Seismic Data. *Journal of Geophysical Research: Solid Earth*.
- Nelson, K. D., Zhao, W., Brown, L. D., Kuo, J., Che, J., Liu, X., ... & Kind, R. (1996). Partially molten middle crust beneath southern Tibet: synthesis of project INDEPTH results. *Science*, 274(5293), 1684-1688.
- Nissen, S. S., Hayes, D. E., Bohlen, P., Diebold, J., Bochu, Y., Zeng, W., & Chen, Y. (1995). Deep penetration seismic soundings across the northern margin of the South China Sea. *Journal of Geophysical Research: Solid Earth*, 100(B11), 22407-22433.
- Pichot, T., Delescluse, M., Chamot-Rooke, N., Pubellier, M., Qiu, Y., Meresse, F., ... & Auxière, J. L. (2014). Deep crustal structure of the conjugate margins of the SW South China Sea from wide-angle refraction seismic data. *Marine and Petroleum Geology*, 58, 627-643.
- Savva, D., Pubellier, M., Franke, D., Chamot-Rooke, N., Meresse, F., Steuer, S., & Auxière, J. L. (2014). Different expressions of rifting on the South China Sea margins. *Marine and Petroleum Geology*, 58, 579-598.
- Schulte-Pelkum, V., Monsalve, G., Sheehan, A., Pandey, M. R., Sapkota, S., Bilham, R., & Wu, F. (2005). Imaging the Indian subcontinent beneath the Himalaya. *Nature*, 435(7046), 1222.
- Shan, B., Xiong, X., Zhao, K. F., Xie, Z. J., Zheng, Y., & Zhou, L. (2016). Crustal and upper-mantle structure of South China from Rayleigh wave tomography. *Geophysical Journal International*, 208(3), 1643-1654.
- Shu, L. S. (2012). An analysis of principal features of tectonic evolution in South China Block. *Geological Bulletin*

of China (in Chinese with English abstract), 31, 1035-1053.

- Smit, J., van Wees, J. D., & Cloetingh, S. (2016). The Thor suture zone: From subduction to intraplate basin setting. *Geology*, 44(9), 707-710.
- Subedi, S., Hetényi, G., Vergne, J., Bollinger, L., Lyon-Caen, H., Farra, V., ... & Gupta, R. M. (2018). Imaging the Moho and the Main Himalayan Thrust in Western Nepal With Receiver Functions. *Geophysical Research Letters*, 45(24), 13-222.
- Sun, A., & Zhao, D. Anisotropic tomography beneath Northeast Tibet: evidence for regional crustal flow. *Tectonics*, e2020TC006161.
- Sutra, E., & Manatschal, G. (2012). How does the continental crust thin in a hyperextended rifted margin? Insights from the Iberia margin. *Geology*, 40(2), 139-142.
- Tannock, L., Herwegh, M., Berger, A., Liu, J., Lanari, P., & Regenauer-Lieb, K. (2020a). Microstructural analyses of a giant quartz reef in south China reveal episodic brittle-ductile fluid transfer. *Journal of Structural Geology*, 103911.
- Tannock, L., Herwegh, M., Berger, A., Liu, J., & Regenauer-Lieb, K. (2020b). The effects of a tectonic stress regime change on crustal-scale fluid flow at the Hejuan geothermal fault system, South China. *Tectonophysics*, 781, 228399.
- Tarayoun, A., Mazzotti, S., & Gueydan, F. (2019). Quantitative impact of structural inheritance on present-day deformation and seismicity concentration in intraplate deformation zones. *Earth and Planetary Science Letters*, 518, 160-171.
- Taylor, B., & Hayes, D. E. (1983). Origin and history of the South China Sea basin. *The tectonic and geologic evolution of Southeast Asian seas and islands: Part 2*, 27, 23-56.
- Wada, I., Behn, M. D., & Shaw, A. M. (2012). Effects of heterogeneous hydration in the incoming plate, slab rehydration, and mantle wedge hydration on slab-derived H₂O flux in subduction zones. *Earth and Planetary Science Letters*, 353, 60-71.
- Wang, T. K., Chen, M. K., Lee, C. S., & Xia, K. (2006). Seismic imaging of the transitional crust across the northeastern margin of the South China Sea. *Tectonophysics*, 412(3-4), 237-254.
- Wang, Y., Fan, W., Zhang, G., & Zhang, Y. (2013). Phanerozoic tectonics of the South China Block: key observations and controversies. *Gondwana Research*, 23(4), 1273-1305.
- Wannamaker, P. E., Evans, R. L., Bedrosian, P. A., Unsworth, M. J., Maris, V., & McGary, R. S. (2014). Segmentation of plate coupling, fate of subduction fluids, and modes of arc magmatism in Cascadia, inferred from magnetotelluric resistivity. *Geochemistry, Geophysics, Geosystems*, 15(11), 4230-4253.
- Watanabe, T. (1993). Effects of water and melt on seismic velocities and their application to characterization of seismic reflectors. *Geophysical Research Letters*, 20(24), 2933-2936.
- Xia, S., Shen, Y., Zhao, D., & Qiu, X. (2015). Lateral variation of crustal structure and composition in the Cathaysia block of South China and its geodynamic implications. *Journal of Asian Earth Sciences*, 109, 20-28.
- Xia, S., Zhou, P., Zhao, D., & Cao, J. (2020). Seismogenic structure in the source zone of the 1918 M7.5 NanAo earthquake in the northern South China Sea. *Physics of the Earth and Planetary Interiors*, 106472.
- Xiong, S. B., Jin, D. M., Sun, K. Z., Zou, Y. S., Fan, X. B., & Du, X. G. (1991). Some characteristics of deep structure of the Zhangzhou geothermal field and its neighbourhood in the Fujian province. *Chinese Journal of Geophysics (in Chinese with English abstract)*, 34, 55-63.

- Xu, H., Qiu, X., Zhao, M., Sun, J., & Zhu, J. (2006). Characteristics of the crustal structure and hypocentral tectonics in the epicentral area of Nan'ao earthquake (M7.5), the northeastern South China Sea, *Science Bulletin*, 51(S3), 83-91.
- Yang, L., Ren, J., McIntosh, K., Pang, X., Lei, C., & Zhao, Y. (2018). The structure and evolution of deepwater basins in the distal margin of the northern South China Sea and their implications for the formation of the continental margin. *Marine and Petroleum Geology*, 92, 234-254.
- Yang, Y., Ritzwoller, M. H., Zheng, Y., Shen, W., Levshin, A. L., & Xie, Z. (2012). A synoptic view of the distribution and connectivity of the mid-crustal low velocity zone beneath Tibet. *Journal of Geophysical Research: Solid Earth*, 117(B4).
- Yan, P., Zhou, D., & Liu, Z. S. (2001). A crustal structure profile across the northern continental margin of the South China Sea. *Tectonophysics*, 338(1), 1–21. [https://doi.org/10.1016/S0040-1951\(01\)00062-2](https://doi.org/10.1016/S0040-1951(01)00062-2).
- Yan, Q., Shi, X., Liu, J., Wang, K., & Bu, W. (2010). Petrology and geochemistry of Mesozoic granitic rocks from the Nansha micro-block, the South China Sea: Constraints on the basement nature. *Journal of Asian Earth Sciences*, 37(2), 130-139.
- Yin, Z. X., Lai, M. H., Xiong, S. B., Liu, H. B., Teng, J. W., & Kong, X. R. (1999). Crustal structure and velocity distribution from deep seismic sounding along the profile of Lianjian-Boluo-Gangkou in South China. *Chinese Journal of Geophysics*, 42(3), 383-392.
- Yuan, X., Sobolev, S. V., Kind, R., Oncken, O., Bock, G., Asch, G., ... & Wylegalla, K. (2000). Subduction and collision processes in the Central Andes constrained by converted seismic phases. *Nature*, 408(6815), 958.
- Zhang, Y., Yao, H., Yang, H. Y., Cai, H. T., Fang, H., Xu, J., ... & Chen, K. X. (2018). 3-D Crustal Shear-Wave Velocity Structure of the Taiwan Strait and Fujian, SE China, Revealed by Ambient Noise Tomography. *Journal of Geophysical Research: Solid Earth*, 123(9), 8016-8031.
- Zhang, Z., & Wang, Y. (2007). Crustal structure and contact relationship revealed from deep seismic sounding data in South China. *Physics of the Earth and Planetary Interiors*, 165(1-2), 114-126.
- Zhao, B., Zhang, Z., Bai, Z., Badal, J., & Zhang, Z. (2013). Shear velocity and Vp/Vs ratio structure of the crust beneath the southern margin of South China continent. *Journal of Asian Earth Sciences*, 62, 167-179.
- Zhao, F., Alves, T. M., Wu, S., Li, W., Huuse, M., Mi, L., ... & Ma, B. (2016). Prolonged post-rift magmatism on highly extended crust of divergent continental margins (Baiyun Sag, South China Sea). *Earth and Planetary Science Letters*, 445, 79-91.
- Zhao, F., Alves, T. M., Xia, S., Li, W., Wang, L., Mi, L., ... & Fan, C. (2020). Along-strike segmentation of the South China Sea margin imposed by inherited pre-rift basement structures. *Earth and Planetary Science Letters*, 530, 115862.
- Zhao, G., & Cawood, P. A. (1999). Tectonothermal evolution of the Mayuan Assemblage in the Cathaysia Block; implications for Neoproterozoic collision-related assembly of the South China Craton. *American Journal of Science*, 299(4), 309-339.
- Zhao, G., & Cawood, P. A. (2012). Precambrian geology of China. *Precambrian Research*, 222, 13-54.
- Zhao, M., Qiu, X., Ye, C., Xia, K., Huang, C., Xie, J., ... & Sun, L. (2004). An Analysis on Deep Crustal Structure Along the Onshore-Offshore Seismic Profile Across the Binghai (Littoral) Fault Zone in NE South China Sea. *Chinese Journal of Geophysics*, 47(5), 954-961.
- Zhao, Z., Sun, Z., Liu, J., Pérez-Gussinyé, M., & Zhuo, H. (2018). The continental extension discrepancy and

anomalous subsidence pattern in the western Qiongdongnan Basin, South China Sea. *Earth and Planetary Science Letters*, 501, 180-191.

Zheng, T., Zhao, L., & Zhu, R. (2009). New evidence from seismic imaging for subduction during assembly of the North China craton. *Geology*, 37(5), 395-398.

Zhou, L., Xie, J., Shen, W., Zheng, Y., Yang, Y., Shi, H., & Ritzwoller, M. H. (2012). The structure of the crust and uppermost mantle beneath South China from ambient noise and earthquake tomography. *Geophysical Journal International*, 189(3), 1565-1583.

Zhou, X. M., & Li, W. X. (2000). Origin of Late Mesozoic igneous rocks in Southeastern China: implications for lithosphere subduction and underplating of mafic magmas. *Tectonophysics*, 326(3-4), 269-287.

Zhu, L. (2000). Crustal structure across the San Andreas Fault, southern California from teleseismic converted waves. *Earth and Planetary Science Letters*, 179(1), 183-190.

Zhu, L., & Kanamori, H. (2000). Moho depth variation in southern California from teleseismic receiver functions. *Journal of Geophysical Research: Solid Earth*, 105(B2), 2969-2980.

Zou, H. (1998). The deep structure and earthquake mechanism of the continental margin seismic belt along the northern south china sea. *South China Journal of Seismology*, 18(3), 16-20.

Declaration of competing interests

The authors declare that they have no known competing financial interests or personal relationships that could have appeared to influence the work reported in this paper.

The authors declare the following financial interests/personal relationships which may be considered as potential competing interests:

Journal Pre-proof

Credit Author Statement

Pengxiang Zhou: Methodology, Validation, Formal analysis, Investigation, Data Curation, Writing - Original Draft, Visualization.

Shaohong Xia: Conceptualization, Formal analysis, Writing - Review & Editing, Supervision, Project administration, Funding acquisition.

György Hetényi: Methodology, Software, Validation, Formal analysis, Investigation, Writing - Review & Editing.

Vadim Monteiller: Methodology, Investigation, Supervision.

Sébastien Chevrot: Formal analysis, Writing - Review & Editing.

Jie Sun: Project administration, Funding acquisition.

Journal Pre-proof

Highlights

- Spatial variation of mid-crustal low-velocity layer revealed by P-to-S receiver functions.
- The low-velocity layer results from fluids produced by dehydration of the paleo-Pacific slab accumulated in the mid-crust.
- The variability of the low-velocity layer may explain the variability of crustal stretching in the northern South China Sea rifted margin.

Journal Pre-proof

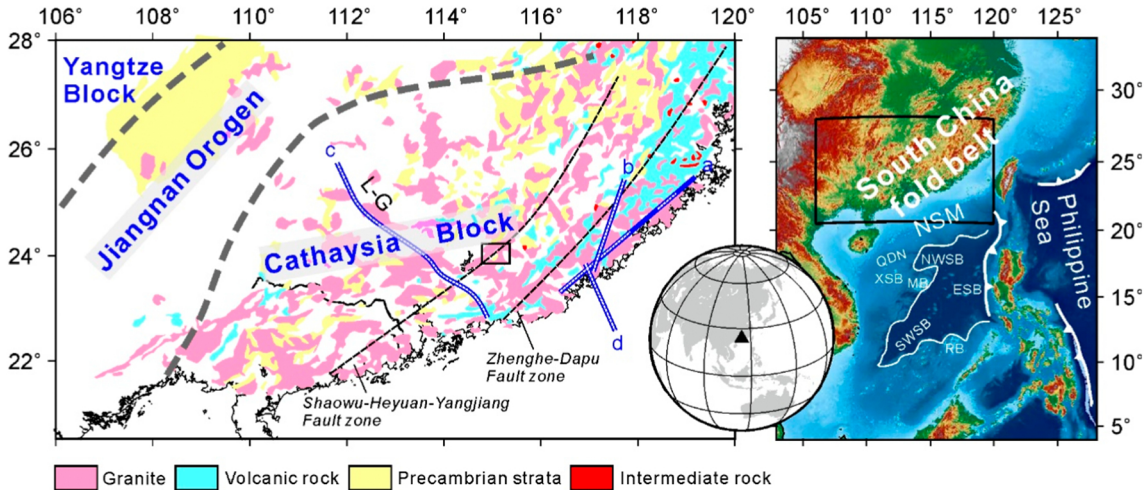


Figure 1

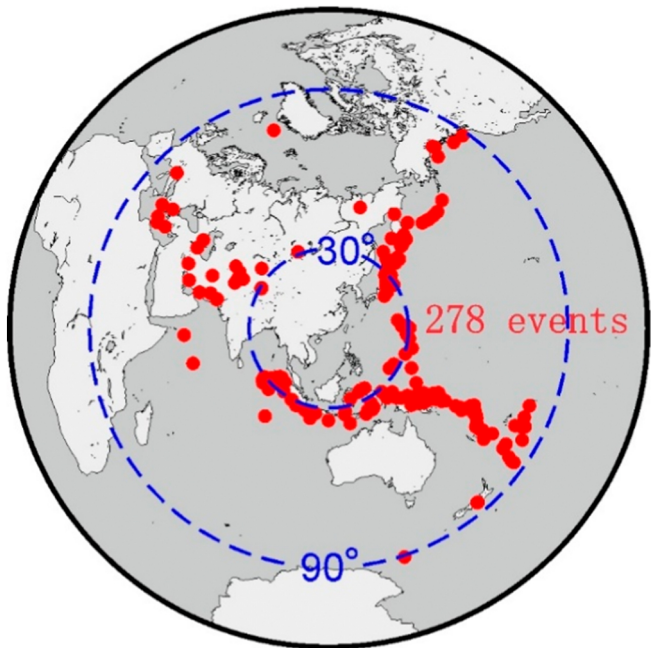


Figure 3

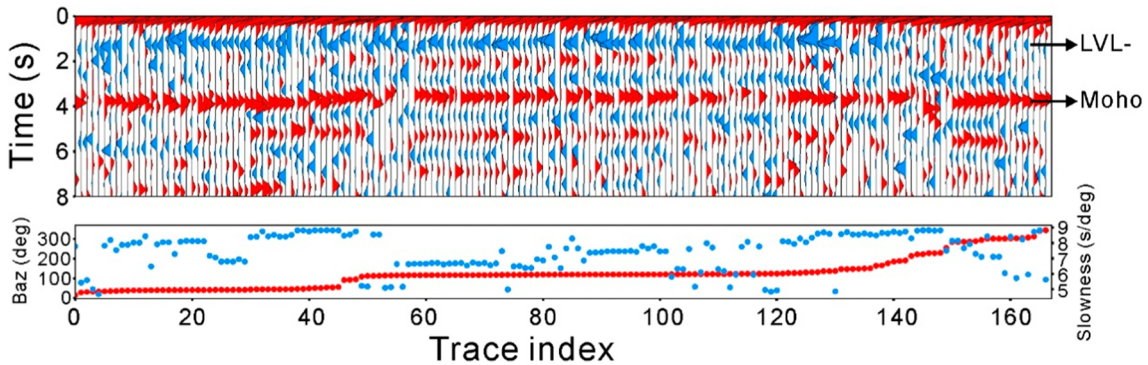


Figure 4

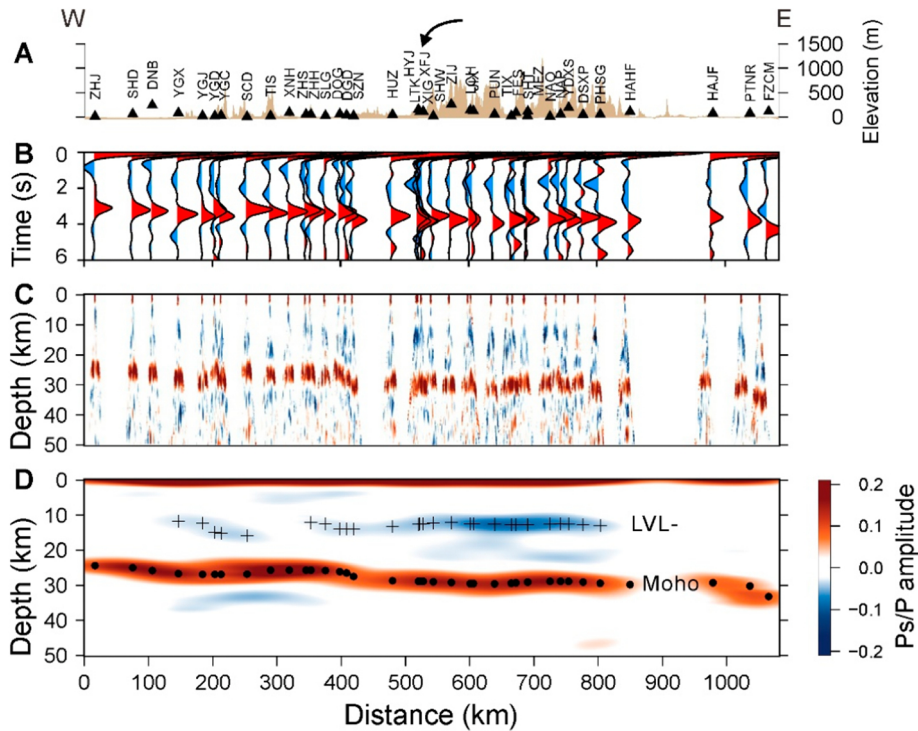


Figure 5

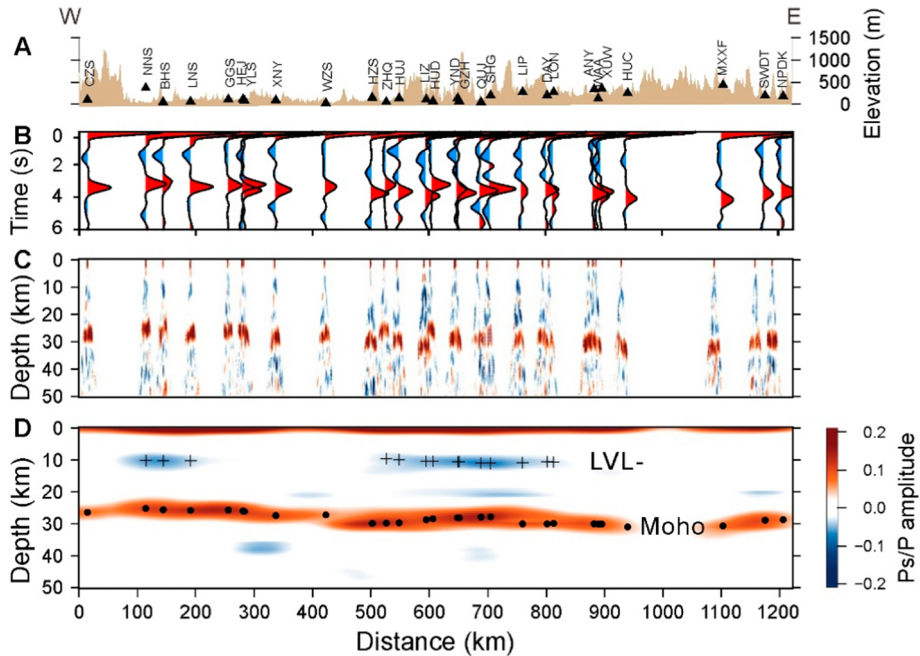


Figure 6

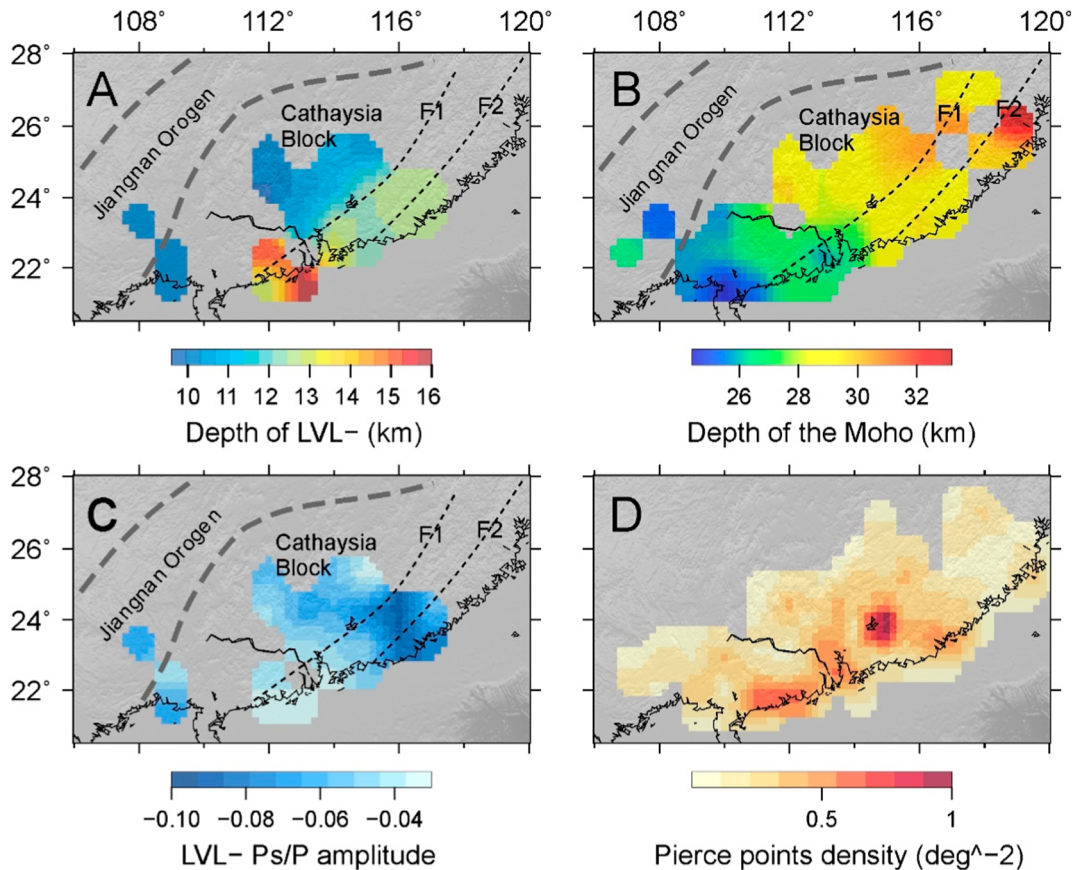


Figure 7

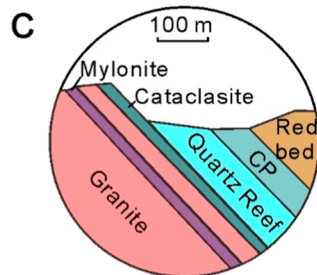
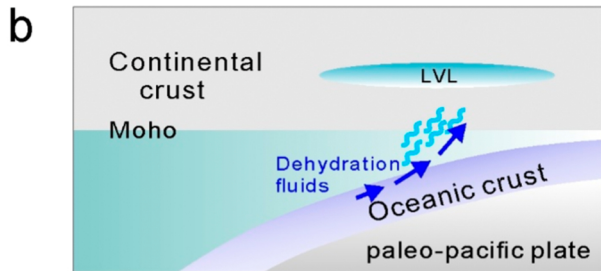
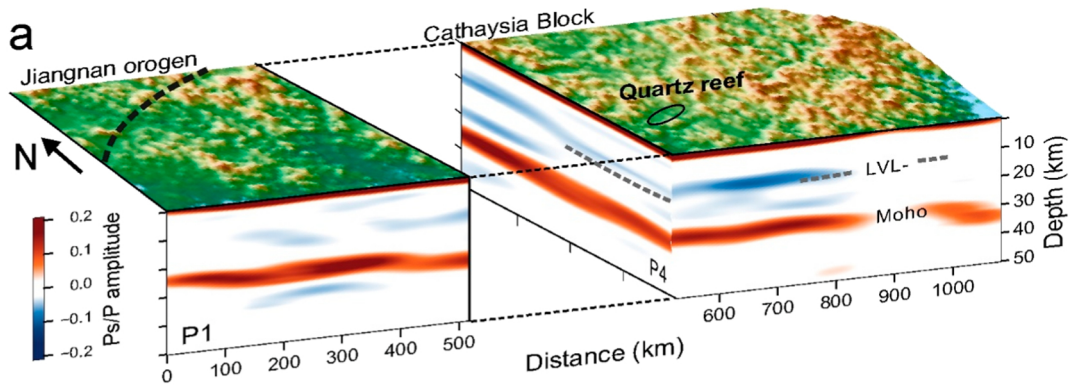


Figure 8

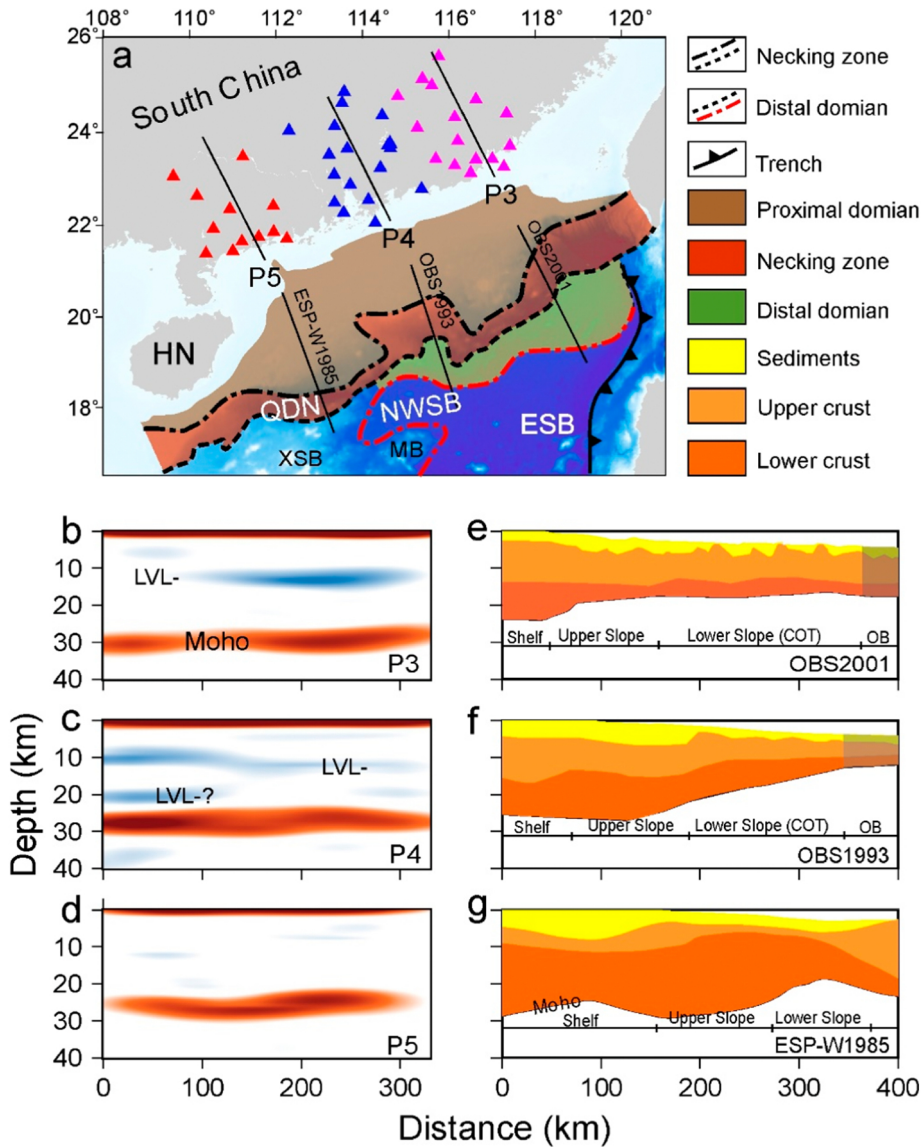


Figure 9